Marine Geology 449 (2022) 106820

Contents lists available at ScienceDirect

Marine Geology

journal homepage: www.elsevier.com/locate/margo

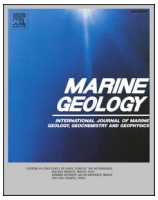

New model for seasonal ikaite precipitation: Evidence from White Sea glendonites

Kseniia Vasileva [a,*], Nataliya Zaretskaya [b], Victoria Ershova [a,c], Mikhail Rogov [c], Lisa D. Stockli [d], Daniel Stockli [d], Vadim Khaitov [e,f], Fedor Maximov [a], Irina Chernyshova [a], Natalia Soloshenko [f], Nikolay Frishman [g], Taras Panikorovsky [a,g], Oleg Vereshchagin [a]

[a] Institute of Earth Sciences, St. Petersburg State University, University Emb. 7/9, 199034 St. Petersburg, Russia
[b] Institute of Geography, Russian Academy of Sciences, Staromonetniy lane, 29, 119017 Moscow, Russia
[c] Geological Institute of RAS, Pyzhevski Lane 7, 119017 Moscow, Russia
[d] University of Texas, Jackson School of Geosciences, 2305 Speedway Stop C1160, Austin, TX 78712-1692, United States of America
[e] Faculty of Biology, St. Petersburg State University, University Emb. 7/9, 199034 St. Petersburg, Russia
[f] Zavaritsky Institute of Geology and Geochemistry, Ural Branch of Russian Academy of Science, 620016 Ekaterinburg, 15 Academika Vonsovskogo str., Russia
[g] Kola Science Center of the Russian Academy of Sciences, 184209, Murmansk district, Apatity, Fersmana Str, 14, Russia

ARTICLE INFO

Editor: Adina Paytan

Keywords:
Ikaite
Glendonite
Calcite generations
Climate
Diagenesis
White Sea

ABSTRACT

The mineral ikaite ($CaCO_3{\cdot}6H_2O$) and its pseudomorphs (glendonite) are considered as important paleoclimate indicators in the geological record. Here we examine the youngest known glendonites, their host concretions, and bivalve shells fossilized within these host concretions from the White Sea, north-western Russia. We applied mineralogical, geochemical and isotopic methods to shed new light on the paleogeographic and geochemical environments during ikaite precipitation and ikaite-calcite transformation. We show that White Sea glendonites are so far the youngest known glendonites in the world (4.1 ± 0.4 cal thousand years before present). Ikaite precipitation occurred during the cold winter months, accompanied by the formation of extensive sea ice and presence of decaying organic matter, which resulted in a small negative Ce anomaly and negative $\delta^{13}C$ values. Increasing temperature led to ikaite dehydration and subsequent cementation with aragonite or amorphous calcium carbonate, containing elevated concentrations of Ba and Sr. Needle-like cements within glendonites display small negative Ce anomalies and precipitated from pore waters derived from seawater. The high-magnesium calcite forming the host concretion precipitated in the sulfate-reduction zone from pore waters derived from seawater. The geochemistry of these pore waters was modified by interaction with clastic components of the host sediments, resulting in $\delta^{18}O$ values comparable to those of dissolved inorganic carbon (DIC) and almost flat Post Archean Australian Shale (PAAS)-normalized rare earth element patterns. Therefore, we show that glendonites can be used as a proxy for near-freezing bottom water temperatures at least seasonally during the cold winter months. Changes in the geochemical composition of carbonate phases within the glendonites and host concretions can be used to determine successive changes in the geochemical environment during their formation.

1. Introduction

Over the past few decades, glendonites (pseudomorphs of the mineral ikaite; $CaCO_3{\cdot}6H_2O$) have attracted a lot of attention among paleoclimatologists due to their potential application as a paleoclimate proxy in the geological past (e.g., Kaplan, 1980; Rogov et al., 2021; Schultz, 2009; Vasileva et al., 2019; Vickers et al., 2018, 2020). In modern marine environments, ikaite precipitates at temperatures of <7 °C, with subsequent dehydration and cementation leading to replacement by anhydrous minerals, mainly calcite. Ikaite has been found in ice (Dieckmann et al., 2008), in marine settings (Domack et al., 2007; Kodina et al., 2001), in caves (Bazarova et al., 2018, 2016, 2014; Bazarova and Kadebskaya, 2019), and in frozen lakes (Last et al., 2013; Whiticar and Suess, 1998). However, ikaite has been precipitated at temperatures of up to 35 °C under controlled laboratory conditions (Tollefsen et al., 2020), which has led some researchers to question the

* Corresponding author.
E-mail addresses: k.vasilyeva@spbu.ru (K. Vasileva), zaretsk@igras.ru (N. Zaretskaya), v.ershova@spbu.ru (V. Ershova), o.vereshchagin@spbu.ru (O. Vereshchagin).

https://doi.org/10.1016/j.margeo.2022.106820
Received 18 March 2022; Received in revised form 7 May 2022; Accepted 9 May 2022
Available online 14 May 2022

formation of ikaite (and subsequently glendonite) as an indicator of cold climates in the geological past. Therefore, further studies are required to better understand the factors controlling the formation of ikaite.

Although discoveries of modern ikaites are abundant (see Rogov et al., 2021 and references therein) and the modern environment of ikaite precipitation is well-known, the origin of ancient glendonites is still debated due to the incompleteness of the geological record and ambiguous paleoclimatic and paleoenvironmental signatures. Glendonites are often associated with glacial dropstones and cold-water faunal assemblages (e.g., Price, 1999; Rogov et al., 2017; Vasileva et al., 2019), supporting assertions of ikaite formation in similar cold-water environments in the geological past to those of the modern. However, although low temperatures undoubtedly play an important role in the formation of ikaite and its transformation into glendonite, the presence of methane seeps in the ikaite formation zone also appears to represent an important prerequisite (Morales et al., 2017; Teichert and Luppold, 2013). To date, comparatively few glendonite studies have been focused on the Holocene (for example, Derkachev et al., 2007; Greinert and Derkachev, 2004; Obzhirov et al., 2000), despite the fact that climate changes of the Holocene are better known than any other interval in the geological past in which glendonites occur. Therefore, a detailed study of Holocene glendonites can provide significant new constraints on the factors controlling the precipitation of ikaite and its subsequent transformation to glendonite.

One of the first discoveries of Holocene glendonites was made in the White Sea near Arkhangel'sk, where they were brought up in fishing nets and termed "White Sea hornlets" (Fedotova et al., 1986; Sokolov, 1825). In 1824, Prof. N. Shcheglov compiled a report on these "hornlets" for the St. Petersburg Mineralogical Society and described them as calcite pseudomorphs replacing aragonite (Jeremejew, 1882). Using crystallographic angles, Prof. P.V. Eremeev mistakenly concluded that celestine formed the primary mineral within glendonites (Jeremejew, 1882). Prof. A.E. Fersman also described White Sea hornlets, along with similar specimens from Spitsbergen, Taimyr and Novaya Zemlya (Fersman, 1938). A resurgence of interest in glendonites appeared after the recognition that glendonites actually represent the pseudomorphs of ikaite (Kaplan, 1979; Suess et al., 1982), and numerous subsequent studies on the White Sea hornlets were published (Fedotova et al., 1986; Geptner et al., 2014, 1994). These studies provide a broad spectrum of data on host sediments, microscopic structure, mineralogical and isotopic composition, but information on their age constraints and paleoenvironmental significance is limited. We aim to fill this gap in knowledge by providing a comprehensive study of the White Sea glendonites, with the aim of determining the precise geochemical environment for their formation and subsequent diagenesis.

2. Geological setting

The modern White Sea forms the portion of the Arctic Ocean that is landlocked between the Kola and Kanin peninsulas. The studied samples were collected from Kandalaksha Bay in the northern part of the White Sea (Fig. 1), which is located on the Baltic Shield and underlain by crystalline Precambrian rocks (Astafiev et al., 2012). In the Kandalaksha Bay area, late Pleistocene glacial deposits unconformably overlie Precambrian basement, while the overlying Holocene strata were deposited in glaciomarine and marine environments (Astafiev et al., 2012). Holocene deposits are represented by light-brown unsorted thinly laminated sands and grey silts, containing occasional pebbles and gravel (Geptner et al., 1994). The coast of Kandalaksha Bay comprises a broad low-angled tidal plain, characterized by very fine-grained sands, silts and muds, with occasional pebbles and boulders.

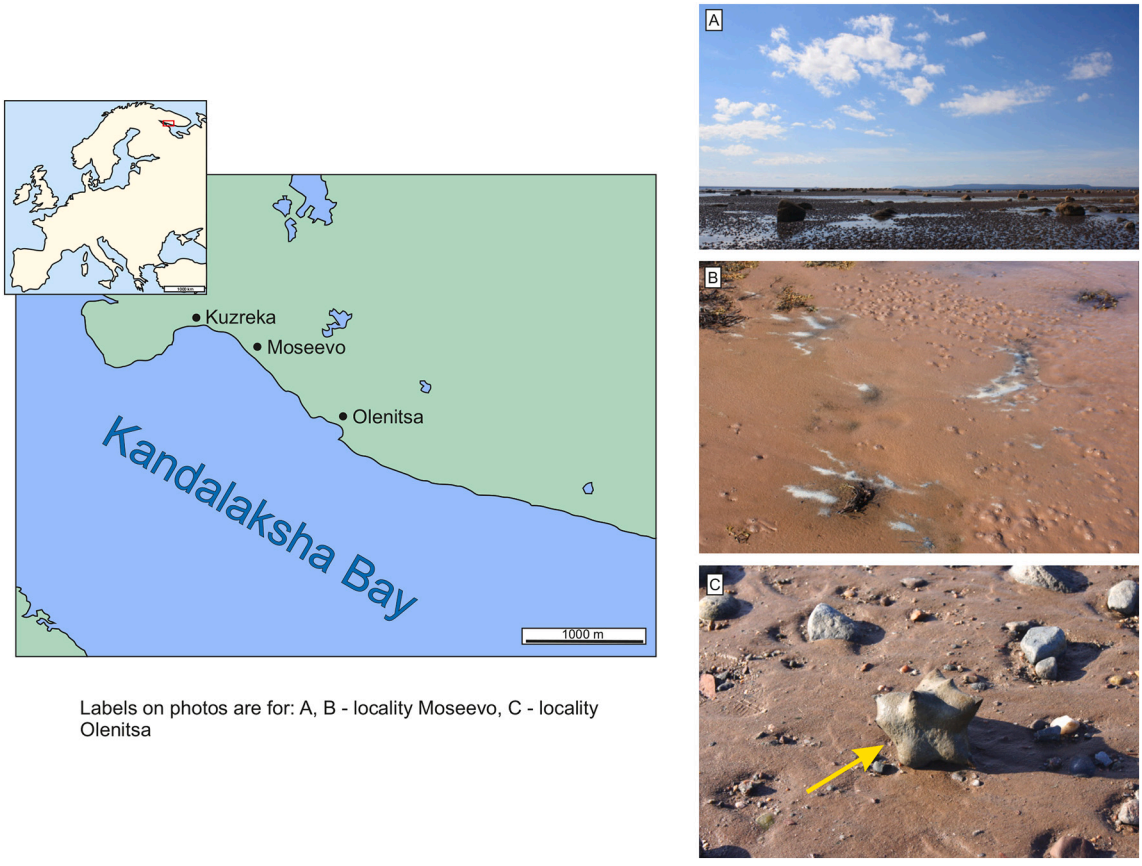

Labels on photos are for: A, B - locality Moseevo, C - locality Olenitsa

Fig. 1. Glendonite sample localities. The yellow arrow in Fig. 1c indicates a glendonite sample (BM-5). (For interpretation of the references to colour in this figure legend, the reader is referred to the web version of this article.)

3. Material and its collection

Twenty five glendonite samples were collected from the eastern coast of Kandalaksha Bay (Fig. 1). Five samples contained bivalve shells, while four samples were embedded in substrate of the host concretion. Glendonite concretions are found within the pyritized mud. Glendonites were collected from three closely spaced localities along the northern coast of Kandalaksha Bay, including Olenitsa, Moseevo and Kuzreka. All of the samples were handpicked from the sediment surface within the littoral zone.

4. Methods

Firstly, each sample was cut in half. Half of the sample was used to prepare polished thin-sections for detailed cathodoluminescence, petrographic (optical and scanning electron microscope), mineralogical (energy dispersive spectroscopy) and geochemical (in situ rare earth element (REE) and trace element) studies, while the other half was used for bulk mineralogical (powder X-ray diffraction), geochemical and isotopic studies.

Petrographic and cathodoluminescence characteristics were studied using a polarizing Olympus BX-53 microscope with a CL8200 Mk-5 Optical cathodoluminescence (CL) system for cold CL, with an accelerating voltage of 6–10 kV and current of 220–250 μA. Micromorphology and elemental composition of minerals were studied at the next stage, using the same thin sections under a Hitachi S-3400 N scanning electron microscope equipped with an Oxford Instruments AzTec Energy X-Max 20 energy dispersive (EDX) spectrometer. The EDX spectra were obtained using a 20 kV accelerating voltage and 1 nA beam current. Trace element analysis of different carbonates found by SEM-EDX was conducted at the laser ablation high-resolution inductively coupled plasma mass spectrometry laboratory at the University of Texas, Austin (UTChron Laboratory, Department of Geological Sciences). The laser ablation (LA) inductively coupled plasma mass spectrometry (ICP-MS) system consisted of a PhotonMachines Analyte.G2 ArF excimer 193 nm laser, equipped with a two-volume Helex sample cell, coupled to a Thermo Element 2 double-focusing magnetic sector ICP-MS. Helium was used as the carrier gas and mixed with argon before entering the ICP-MS. All analyses were conducted on polished thin sections with a laser beam diameter of 50 μm, operated with an energy density of 2.0 J/cm^2, measured with an energy meter and a pulse rate of 8 Hz. Each analysis consisted of 2 cleaning shots, 25 s of baseline data collection, 20 s of ablation and 30 s of washout. NIST612 was used as the primary reference material and GSE-1G basalt glass for quality control. The stoichiometric concentration of calcium in calcite (40.04%) was used for internal standardization of elemental concentrations. Data reduction utilized the Trace Element_IS data reduction scheme in Iolite (Woodhead et al., 2007). Concentrations of REE were normalized to Post-Archean Australian Shale (PAAS; Taylor and McLennan, 1985). Anomalies of Eu, Ce and Y were quantified using equations given in Bau and Dulski (1996), Bau and Alexander (2006) Ponnurangam et al. (2016).

For bulk mineralogical, geochemical and isotopic analyses, samples were extracted using a microdrill. Mineralogical composition was studied using a Rigaku Miniflex II diffractometer, with CuKα radiation, 2°/min scan speed, and a 2-theta of 5–120°. Relative phase proportions were determined using the Rigaku PDXL v. 2.0 software. Major elements (Ca, Mg, Mn and Fe) were studied with ICP atomic emission spectroscopy (AES) using an Optima 8000 DV (Perkin Elmer). Trace elements were determined using a quadrupole ICP-MS NexION 300S (Perkin Elmer). Powdered samples weighing 0.1–1.5 g were leached for 30 min in 0.01 M HCl, then once the probes were separated from the insoluble residue in the centrifuge, they were leached in 2.5 ml of 0.1 N HCl and 3.5 ml of 1 M HCl. The probes were then evaporated and leached in 3% HNO_3. Chemical analyses were made on 50 ml of solution. Stable oxygen and carbon isotopes were analyzed using the Thermo electron system, including a Delta V Advantage Mass Spectrometer with Gas-Bench-II. Analytical precision for both $\delta^{18}O$ and $\delta^{13}C$ was ±0.2‰ (Zaitsev and Pokrovsky, 2014). Sr isotope measurements were carried out using a MC ICP-MS Neptune Plus equipped with an ASX 110 FR sample introduction system, fitted with a PFA micro-flow nebulizer (50 μl/min) connected to a quartz spray chamber. The $^{87}Sr/^{86}Sr$ ratio was normalized by the value of $^{88}Sr/^{86}Sr = 8.37861$. Normalized values were corrected by bracketing every two samples with the SRM-987 standard and correcting to the reference SRM-987 standard value of 0.710245 (Jochum et al., 2005). Analytical precision for the $^{87}Sr/^{86}Sr$ measurements was ±0.003%.

We used the $^{230}Th/U$ dating method to determine the ages of the glendonites. Four sub-samples of the host concretion with glendonite were radiochemically analyzed using the "total sample dissolution" (TSD) technique (Bischoff and Fitzpatrick, 1991; Maksimov and Kuznetsov, 2010). To exclude the influence of contamination with ^{232}Th from clastic components, isochrons were plotted (Bischoff and Fitzpatrick, 1991; Geyh, 2008; Rowe and Maher, 2000). Radiometric measurements of U and Th isotopes were carried out on an ORTEC's Alpha Suite Alpha Spectrometer at The Laboratory of Geomorphology and Paleogeography of Polar Regions and the World Ocean, St. Petersburg State University, Russia. Normalization of the analytical isotopic data against ^{232}Th allowed us to build linear isochrons using $^{230}Th/^{232}Th$ – $^{234}U/^{232}Th$ and $^{234}U/^{232}Th$ – $^{238}U/^{232}Th$ coordinates, as well as calculate the $^{230}Th/^{234}U$ and $^{234}U/^{238}U$ activity ratios and age of the carbonate fraction, based on methods given in Geyh (2008) and Maksimov and Kuznetsov (2010).

5. Results

5.1. Glendonite morphology and bivalve shell identification

We identified four morphological types of glendonite based on our optical studies, including rosette (15 samples), bladed (4 samples), three-pointed (4 samples) and four-pointed glendonites (2 samples).

Rosette glendonites are the most abundant of the four glendonite morphologies and are often found within concretions and associated with large thick-walled bivalve shells (3–5 cm long axis; Figs. 2–6). Two samples (Fr-1 and Fr-4) occurred as overgrowths on granite and serpentinite pebbles, although the glendonites did not pierce the substrate and were easily removed from it. In addition, 5 carbonate concretion samples with bivalve shells were studied. The bivalves *Mya truncata* (Linnaeus), *Macoma calcarea* (Gmelin), *Hiatella arctica* (Linnaeus), *Tridonta borealis* (Schumacher) and *Thyasyra gouldi (?)* (Philippi) were identified in the concretions (Table 1S; Supplementary Material; Fig. 3).

5.2. Mineralogy and optical studies

Powder X-ray diffraction (PXRD) analyses reveal that the studied samples are mainly composed of calcite (Table S2; Supplementary Material; Fig. 4), with quartz and plagioclase as minor constituents. It is worth noting that the PXRD patterns provide evidence for two calcite generations, which differ significantly in their unit cell parameters. The first generation (calcite-1) is characterized by a sharp diffraction maximum at ~34.4° 2-theta (Fig. 4) and comprises almost pure $CaCO_3$ based on its unit cell parameters. The second generation (calcite-2) has a more diffuse diffraction maximum at ~34.8° 2-theta (Fig. 4), which could indicate the amalgamation of several diffraction maxima (e.g., several calcite generations with different compositions). Smaller unit cell parameters indicate that calcite-2 has a higher content of smaller cations (e.g., Mg, Fe) compared to Ca. Calcite-1 occurs exclusively within glendonites, while calcite-2 can be found within both glendonites and the host concretions. Shells are composed of aragonite.

We distinguished three calcite types based on our optical and SEM studies (for detailed petrography of glendonites see Huggett et al., 2005; Greinert and Derkachev, 2004). The first calcite type comprises dark isometric (rectangular) or elongated tabular crystals, which sometimes group to form aggregates. These crystals are light in colour with 2 or 3

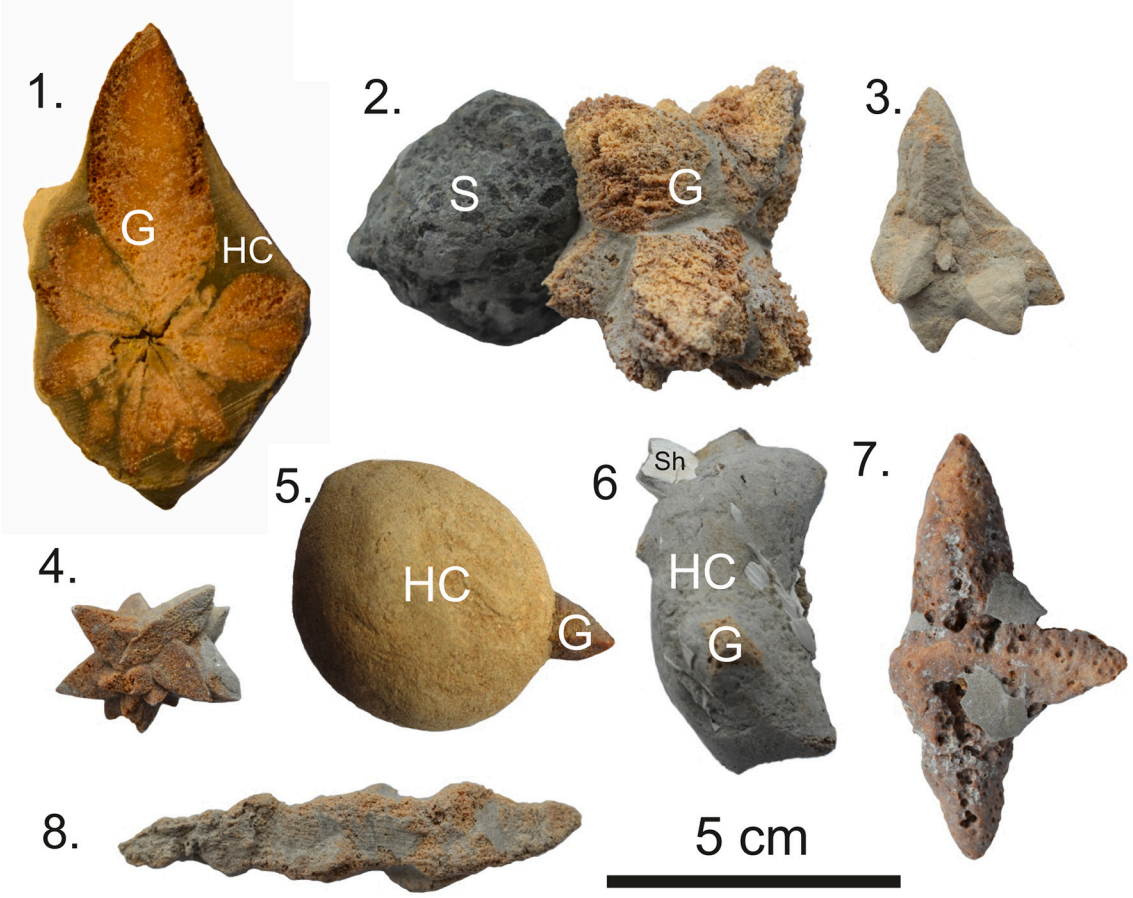

Fig. 2. Morphology of the studied samples. 1–4: rosette glendonites (1 – Ol-5; 2 – Fr-4; 3 – Fr-10; 4 – Fr-8); 5–6: glendonite samples in concretions (5 – Fr-12; 6 – Fr-6); 7: three-pointed glendonite (Fr-15), 10), 8 – stellate-like glendonite (Fr-1). Abbreviations: G – glendonite, HC – host concretion, Sh – shell, S – substrate.

Table 1
Results of the radiochemical analyses of five sub-samples determined by the TSD (total sample dissolution) technique.

No	^{238}U	^{234}U	^{230}Th	^{232}Th	$^{230}Th/^{234}U$	$^{234}U/^{238}U$
	dpm/g*					
798 g	12.177 ± 0.265	14.297 ± 0.305	0.851 ± 0.040	0.265 ± 0.021	0.060 ± 0.003	1.174 ± 0.017
798 h	7.802 ± 0.155	9.041 ± 0.176	0.649 ± 0.034	0.223 ± 0.019	0.072 ± 0.004	1.159 ± 0.018
Fr-5	6.263 ± 0.136	7.277 ± 0.154	0.554 ± 0.022	0.242 ± 0.014	0.076 ± 0.003	1.162 ± 0.021
Fr-8	2.950 ± 0.079	3.540 ± 0.091	0.405 ± 0.018	0.209 ± 0.013	0.114 ± 0.006	1.200 ± 0.033
Fr-14	3.277 ± 0.094	3.763 ± 0.104	0.552 ± 0.029	0.256 ± 0.019	0.147 ± 0.009	1.148 ± 0.033

Note: * - dpm/g - decay per minute per gram.

zones (Fig. 5A) and are non-luminescent (Fig. 5B). The crystals are matrix-supported and comprise 15–20% of the glendonite, ranging in size between 50 and 400 μm (with an average of 100–200 μm). We suggest that this calcite type corresponds to calcite-1 revealed by PXRD.

The second calcite type comprises micritic calcite which appears grey in plane polarized light and constitutes 15–20% of the glendonite, forming curvy lines between crystals of the first calcite type (Fig. 5A, C). This calcite does not form overgrowths on the first calcite type but likely represents the infill of pore space remaining after crystallization of the first calcite generation. We suggest that this calcite type corresponds to calcite-2 revealed by PXRD.

The third calcite type comprises yellowish needle-like, botryoidal or bladed rims 10–20 μm in width, forming overgrowths on both the first and second calcite types. Both the second and third calcite types are characterized by a homogeneous dull-red cathodoluminescence or are non-luminescent (Fig. 5B). In sample Fr-6, a bivalve shell fossilized in the glendonite concretion has been overgrown by bladed calcite crystals of the third calcite type with a dull-red cathodoluminescence, while the bivalve shell itself displays a laminar green cathodoluminescence (Fig. 5A, B). We assume that this calcite type also corresponds to calcite-2 revealed by PXRD.

The host concretions are composed of quartz sandstone with a calcite cement (Fig. 5A, B). Quartz grains are typically 50–100 μm in diameter, angular in shape, with a blue, green or red cathodoluminescence. The calcite cement is micritic and dark brown in plane polarized light, with a dark red or no cathodoluminescence. Occasional small (up to 200 μm in length) thin shell clasts (non-luminescent) appear in concretions. There are equal proportions of quartz/plagioclase grains and calcite cement in the concretions, which explains the quartz and plagioclase revealed by PXRD.

5.3. Scanning electron microscopy and microprobe analyses

Scanning electron microscopy and microprobe analyses reveal that glendonites are composed of two calcite generations. The first calcite type is low-magnesium (less than 1.0 wt% MgO; Fig. 6) with tabular or rosette-like crystals, clearly corresponding to calcite-1 revealed by

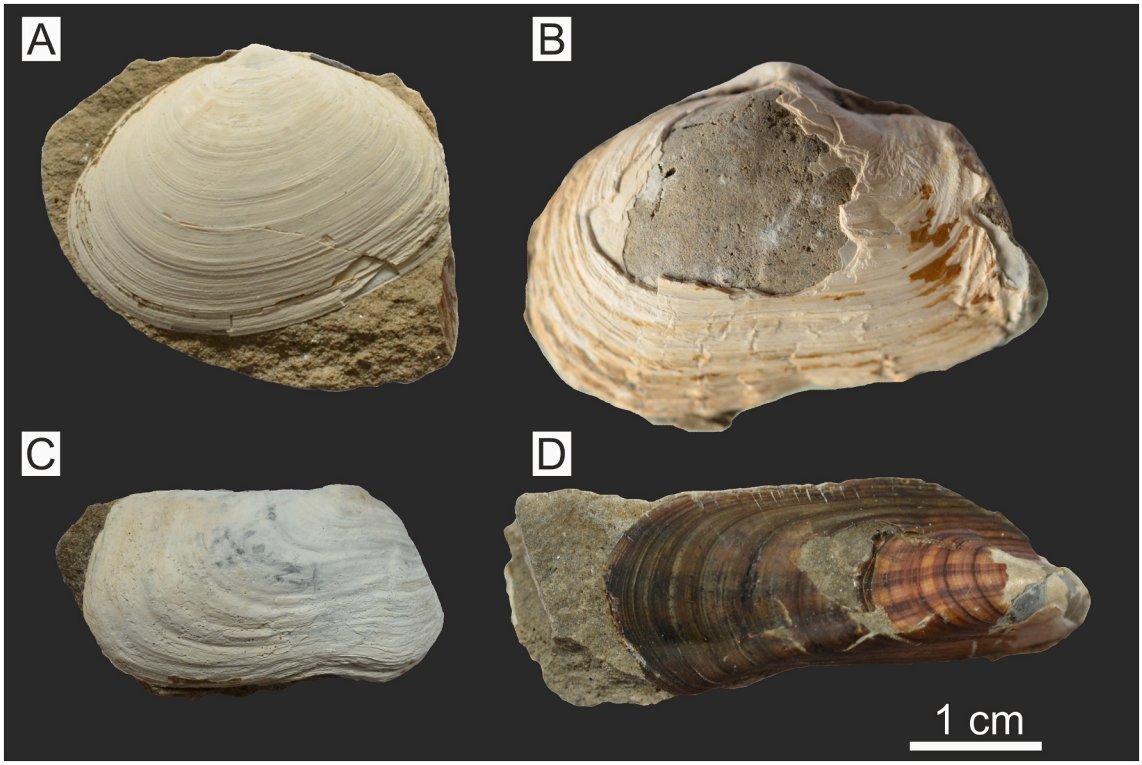

Fig. 3. Photographs of White Sea bivalve shells from the studied concretions: A – *Macoma calcarea* (Gmelin), B – *Mya truncata* (Linnaeus), C – *Hiatella arctica* (Linnaeus), D – *Mytilis* sp.

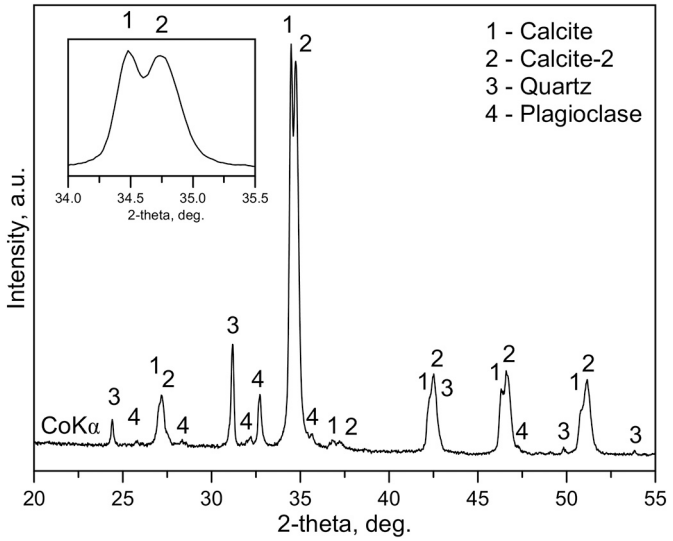

Fig. 4. PXRD-spectra of a representative glendonite sample with a double calcite peak (Sample Ol-4).

PXRD. The second calcite type is high-magnesium (3–4 wt% MgO) and P-rich (1–2 wt% P_2O_5), corresponding to calcite-2 revealed by PXRD. The second calcite type also cements quartz grains in the concretion. Layered silicates and framboidal pyrite (Fig. 6, right) were revealed by our SEM-EDX analyses in addition to calcite, quartz and plagioclase. The third calcite type revealed by optical microscopy is indistinguishable from the second type under SEM.

5.4. Bulk geochemistry

ICP-AES and ICP-MS studies reveal that the glendonites are characterized by a low content of insoluble residue (up to 10%; mean value = 4%), low Mg/Ca ratios (up to 0.082; Table 2S; Supplementary Material), Sr contents ranging from 1100 to 1800 ppm, Mn/Sr ratios ranging from 0.013 to 0.134, and Fe/Sr ratios ranging from 0.029 to 0.877. Samples display an enrichment in heavy REE, low negative Ce/Ce* anomalies (0.8–0.9), low positive Eu anomalies (1.1–1.5), and Y/Ho ratios of 25–38 (Table 3; Fig. 7).

5.5. Carbonate generations geochemistry

LA-ICP-MS results are displayed in Fig. 8 and Table 3S (Supplementary Material). Ikaite-derived calcite, needle-like cement, host concretion calcite and bivalve shells all exhibit distinct PAAS-normalized REE patterns. Host concretion calcite cements display almost flat patterns (Fig. 8; yellow lines), while bivalve shells display significant Ce/Ce* anomalies (0.3; Fig. 8; dark red lines), small Gd/Gd* (1.3–2.0) and Y (1.4–2.5) anomalies, and Y/Ho ratios between 38 and 68 (Fig. 9; right). Ikaite-derived calcite and needle-like calcite cement are characterized by very similar REE concentrations and normalized patterns (Fig. 8; green and blue lines), with a small negative Ce anomaly (0.8–0.9), depletion in light REE (LREE) and heavy REE (HREE), and low Y/Ho ratios (23–44). The differences in Ba and Sr concentrations were also determined (Fig. 9; left). Ikaite-derived calcite has lower concentrations of Ba (0.5–46 ppm) and Sr (330–500 ppm), while the needle-like calcite cement has higher Ba (118–270 ppm) and Sr (617–920 ppm) concentrations. The highest Ba concentrations are found in the host concretion calcite (318–352 ppm), accompanied by Sr concentrations between 814 and 840 ppm. The bivalve shells are characterized by low Ba concentrations (5–12 ppm) and a wide range of Sr concentrations (210–730 ppm) (Fig. 9; right).

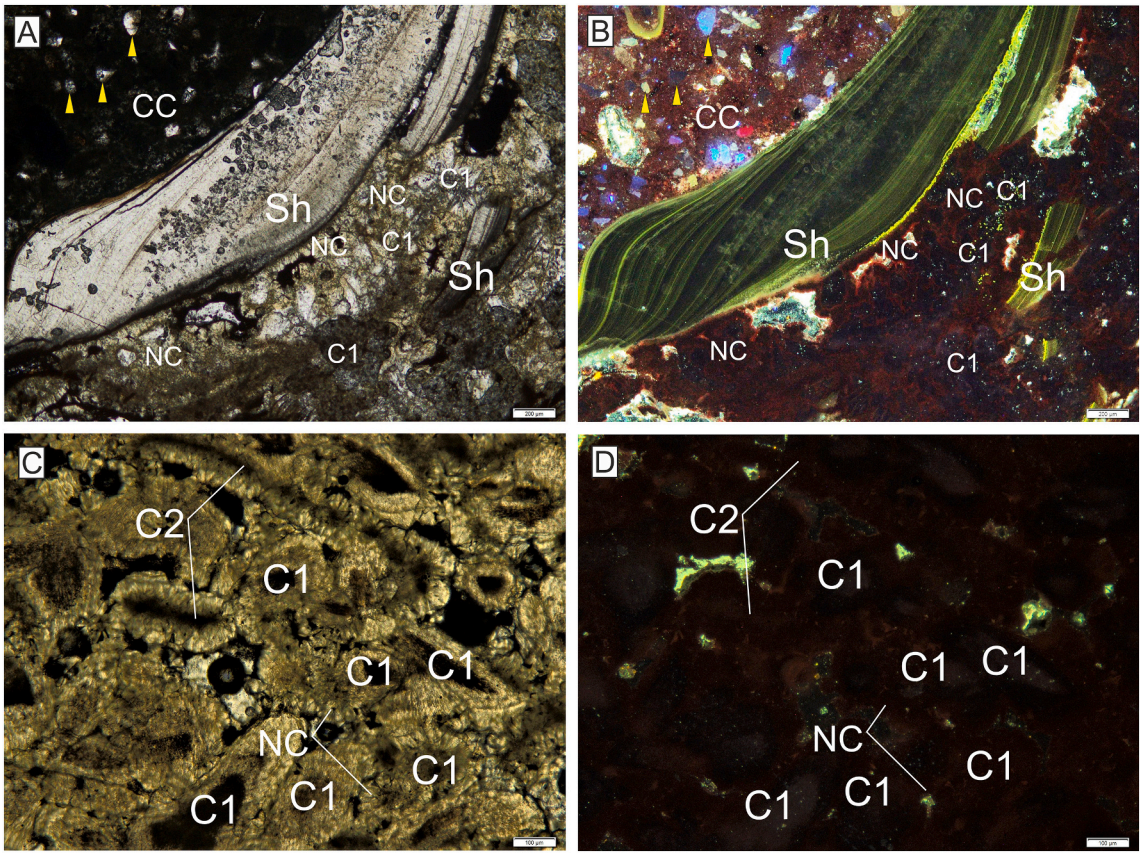

Fig. 5. Optical characteristics of the studied glendonites and concretions. A – sample Fr-6 in plane-polarized light; B – the same in CL. Sh – bivalve shell, C1 – calcite of the 1st generation (ikaite-derived calcite), NC – needle-like cement, CC – concretion cement, detrital quartz grains indicated by yellow arrows. C – sample Fr-14 in plane-polarized light; D – the same in CL. C1 – calcite of the 1st generation (ikaite-derived calcite), NC – needle-like cement. (For interpretation of the references to colour in this figure legend, the reader is referred to the web version of this article.)

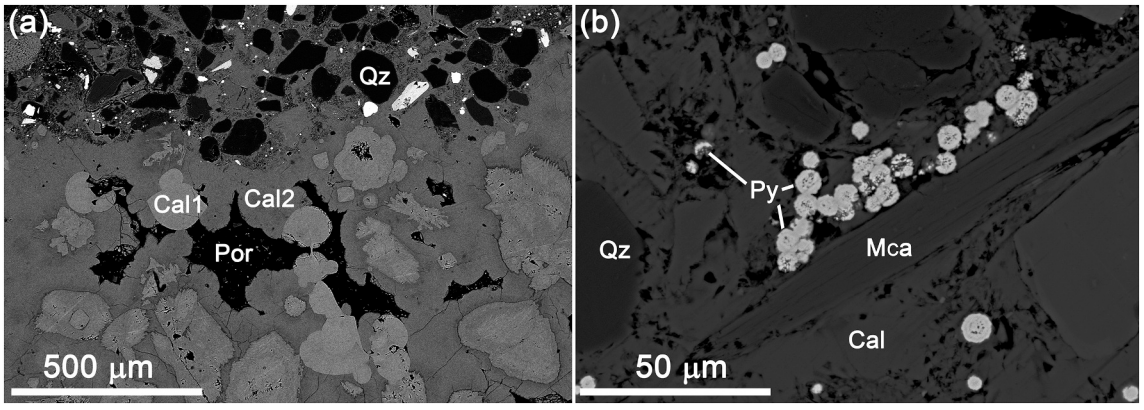

Fig. 6. Backscattered electron (BSE) images of sample Fr-6. Cal1 – low-magnesium calcite, Cal2 high-magnesium calcite, Qz - quartz, Py - pyrite, Mca - mica, Por - pore space.

5.6. $^{230}Th/U$ dating

The results of four leachates of total dissolved glendonite sample are presented in Table 1 and Fig. 10. All samples contain some ^{232}Th, indicating an influence of clastic material on their chemical and isotopic composition. A linear regression was constructed for 4 carbonate subsamples, giving an isochronous age of the carbonate fraction of 4.1 ± 0.4 thousand years.

5.7. Oxygen, carbon and strontium isotopes

Stable oxygen and carbon isotope data are presented in Table 4S (Supplementary Material) and Fig. 11. $\delta^{13}C$ of the glendonite samples ranges from −31.3 to −15.5‰ V-PDB, while $\delta^{18}O$ ranges from −0.4 to −2.1‰ V-PDB. The bivalve shells yielded $\delta^{18}O$ values of −1.4‰ V-PDB and $\delta^{13}C$ values of −1.4‰ V-PDB. Our data sit within the range of published data (Geptner et al., 2014) on the stable isotopic composition of White Sea glendonites (Fig. 11). $^{87}Sr/^{86}Sr$ ratios range from 0.709209 to 0.709299 (Table 3S; Supplementary Material).

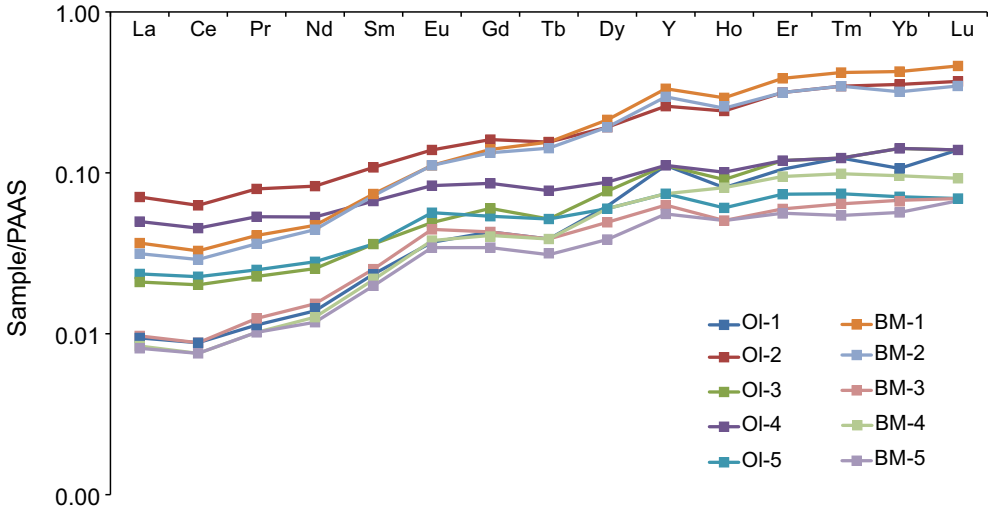

Fig. 7. PAAS-normalized REE patterns of bulk glendonites determined by ICP-AES and ICP-MS.

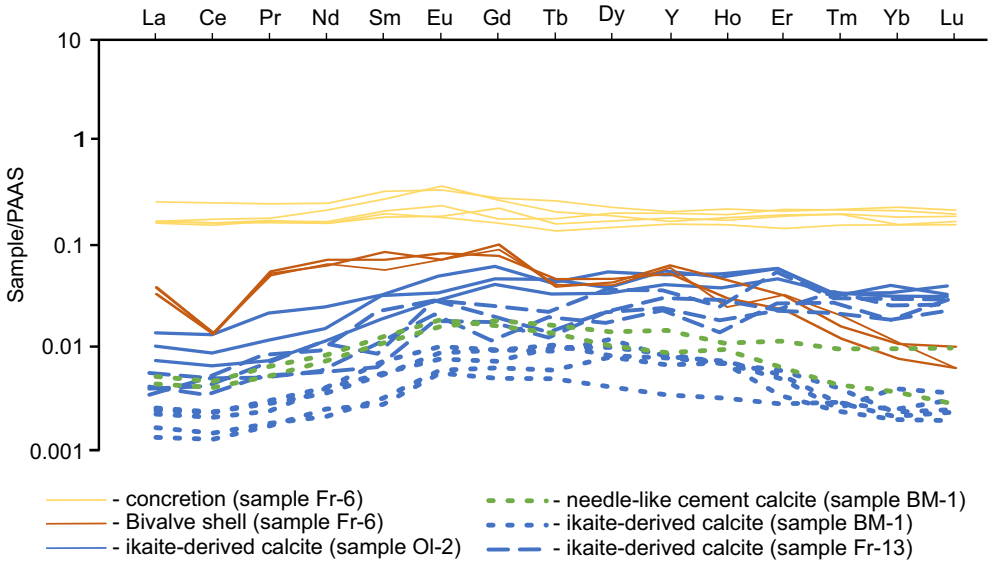

Fig. 8. PAAS-normalized patterns of different calcite types determined by LA-ICP-MS.

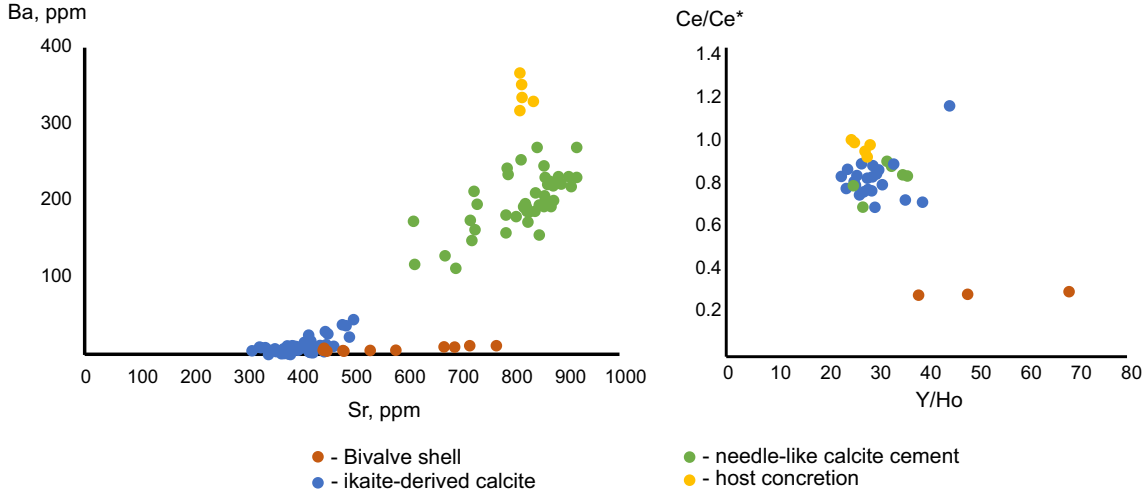

Fig. 9. Sr – Ba and Y/Ho – Ce/Ce* cross-plots based on LA-ICP-MS data.

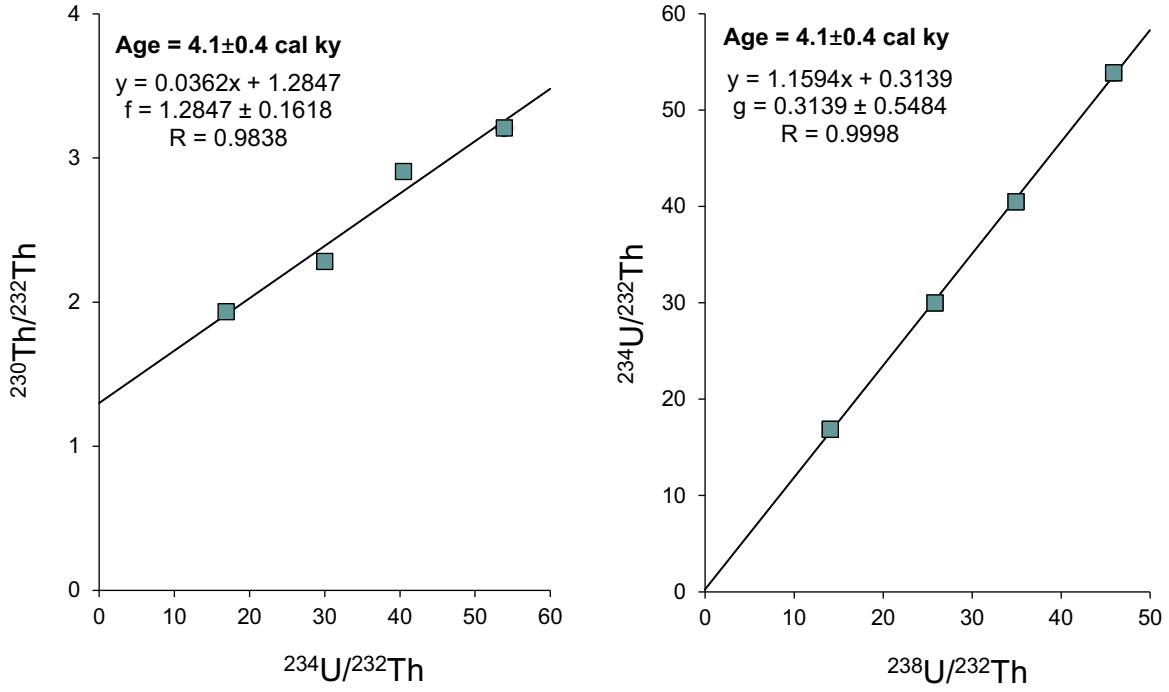

Fig. 10. Left: [$^{234}U/^{232}Th$] versus [$^{230}Th/^{232}Th$] cross plots for the studied glendonite samples of the White Sea; right: [$^{234}U/^{232}Th$] versus [$^{238}U/^{232}Th$] cross plots for the studied glendonite samples of the White Sea. The intercept on the Y-axis in the plots of $^{230}Th/^{232}Th$ vs $^{234}U/^{232}Th$ and $^{234}U/^{232}Th$ vs $^{238}U/^{232}Th$ isotope activity gives the values correction indexs f and g required for defining the clastic-free (that is, in the carbonate fraction) $^{230}Th/^{234}U$ and $^{234}U/^{238}U$ activity ratios for the four coeval samples. The isochronous age calculated from these activity ratios is 4.1 ± 0.4 kyr.

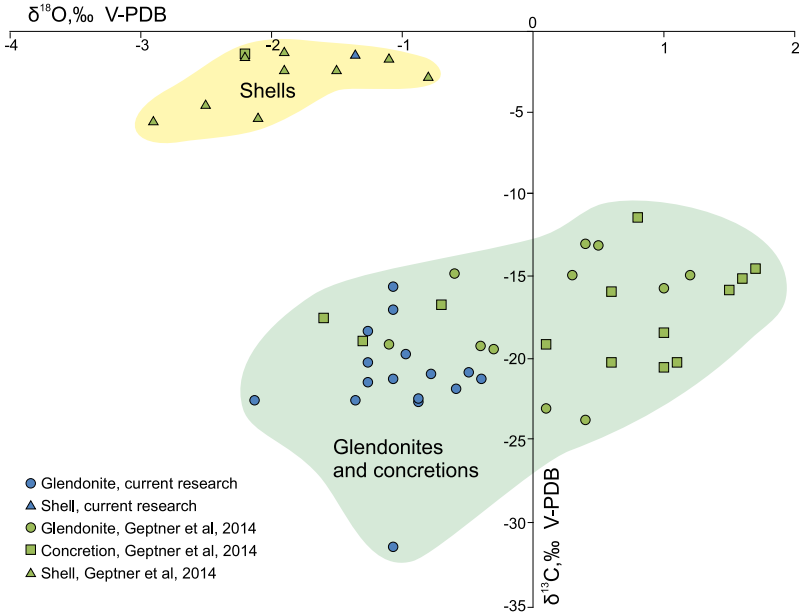

Fig. 11. $\delta^{18}O$ vs. $\delta^{13}C$ cross-plot for glendonites and bivalve shells.

6. Discussion

6.1. Age constraints, temperature and water depth of ikaite precipitation

The Holocene climatic evolution of the White Sea area has been studied in detail and is well constrained (e.g., Agafonova et al., 2020; Naumov, 2006; Novichkova et al., 2017 among others). Deglaciation of the White Sea ended at about 12.8 cal ka BP (calibrated thousand years before present) (Hughes et al., 2016; Lavrova, 1960). Since the end of the late Pleistocene, cold (stadial) and warm (interstadial) periods have been detected in the study region, including the Bølling–Allerød interstadial, Younger Dryas stadial, Preboreal, Boreal, Atlantic, Subboreal and Subatlantic stages (Naumov, 2006). The history of the White Sea development was elaborated by Koshechkin (1979), and the stages of its transgressions and regressions were determined such as Portlandia (Late Glacial transgression), Littorina regression, Tapes mid-Holocene transgression, and Trivia and Ostrea regressive stages (Koshechkin, 1979). This reconstruction was then developed by Kolka et al. (2013) and many other scientists (Subetto et al., 2012; Repkina et al., 2018, etc.).

The age of the White Sea glendonites was previously determined

using the ^{14}C-method as 10,140 ± 150, 9440 ± 186 and 9630 ± 250 years (Geptner et al., 1994), i.e., 11.25–9.83 cal ka BP. However, the typical bivalve assemblage (*M. truncata* Linnaeus, *M. calcarea* Gmelin, *H. arctica* Linnaeus, *T. borealis* Schumacher (?), *Thyasyra gouldi* (?) Philippi; Table 1S) found within glendonite-bearing concretions are characterized by thick walls and span the time interval from 6.9–6.3 cal ka BP in the White Sea (Zaretskaya et al., 2021, 2020), during the warmer climate of the middle Holocene (Atlantic stage). The bivalve shells of the Atlantic stage were larger and thicker than modern specimens (Govberg, 1970, 1968; Naumov, 2006; Nevessky et al., 1977), inhabiting sublittoral environments at 5–20 m depth in cold seas with low salinity (16–30‰) (Naumov, 2006). Strontium isotopic composition of the studied glendonites is very close to modern seawater ratio (e.g. McArthur et al., 2001), but probably is not useful for precise glendonite dating as for the Phanerozoic samples ^{87}Sr/^{86}Sr data does not provide accuracy better than ±3 m.y. (El Meknassi et al., 2018). Our ^{230}Th/U age data suggest that the glendonite pseudomorphs formed around 4.1 ± 0.4 cal ka BP (Subboreal stage of the Holocene), indicating that the glendonites are younger than the bivalves. While the bivalves date from the warm Atlantic stage, the age of the glendonites (4.1 ± 0.4 cal ka BP) suggests that ikaite precipitation occurred during the Subboreal stage of the Holocene. This stage was marked by a cooling event, when the surface temperature of the White Sea was about 1–2 °C lower than the Atlantic stage and about 3–4 °C higher than the modern (Novichkova et al., 2017).

The isotopic and geochemical data obtained from bulk glendonites are characteristic of almost unaltered marine glendonites. PAAS-normalized REE patterns show negative Ce anomalies (0.8–0.9), suggesting a lack of subsequent overprinting by diagenetic fluids in a redox environment. Therefore, bulk glendonite calcite preserves a primary marine geochemical signal and can be used to calculate crystallization temperature estimates using the equation of Kim and O'Neil (1997). As it was shown by Greinert and Derkachev (2004) and confirmed by Krylov et al. (2015) calcite equilibration formula (Kim and O'Neil, 1997) can be used for temperature calculations of ikaite and calcite pseudomorph. The results of these calculations are presented in Table 4S (Supplementary Material). To calculate our seawater temperatures from primary glendonite calcite and bivalve shells, we used a seawater δ^{18}O value of −4‰ Vienna Standard Mean Ocean Water (V-SMOW) (Geptner et al., 1994). Temperatures calculated from the δ^{18}O values of glendonite calcite range from −3.1 to +5 °C (one glendonite sample shows temperature as high as +8 °C), while temperatures calculated from the δ^{18}O values of bivalve shells range from +3 to +11 °C. The temperatures calculated from isotopic composition of glendonites fits in natural environment of ikaite findings in modern settings (Greinert and Derkachev, 2004; Zabel and Schulz, 2001 among others). The difference in calculated temperatures between the glendonites and bivalve shells is likely to indicate precipitation during both different seasons and different climatic episodes. As it was shown for modern mollusks, their growth rate is limited by temperature-linked metabolic constraints across most latitudes (Killam and Clapham, 2018). Thus, the most plausible explanation of different isotopic composition is that the growth of the bivalve shells in the White Sea occurred in the warm summer months during the warmer Atlantic stage, while the precipitation of ikaite occurred during the cold winter months during the cooler Subboreal stage (See Figs. 12 and 13.)

The water depth of the White Sea in the study region around 4–4.5 cal ka BP has been estimated as 15–20 m (Kolka et al., 2013). In the modern White Sea, summer warming penetrates to a water depth of 15 m (Berger et al., 2003; Fig. 12). Therefore, all of the coastal waters in the study area were warmer during the summer months than the maximum temperature at which ikaite precipitation occurs, and warmer than temperature estimates calculated from δ^{18}O values of the glendonites (Fig. 12).

6.2. Geochemical environment of ikaite precipitation and transformation

The geochemical environment of ikaite precipitation and transformation to calcite can be estimated using changes in chemical composition of the calcite generations determined by our SEM EDX and LA-ICP-MS analyses. These data can also be helpful when studying the fractionation of major and trace elements.

The geochemical environment during the warm summer months in the shallow water littoral environment (5–20 m) was oxic, which is confirmed by the low negative Ce anomaly (0.3) in PAAS-normalized REE patterns of the bivalve shells. The aragonitic bivalve shells do not incorporate Ba and HREE but do incorporate Sr and Y (Y/Ho ratio ranges between 38 and 68), indicating direct precipitation from seawater.

We propose that ikaite crystallization occurred on the seafloor or in highly flooded sediment layer as in some cases ikaite is attached to

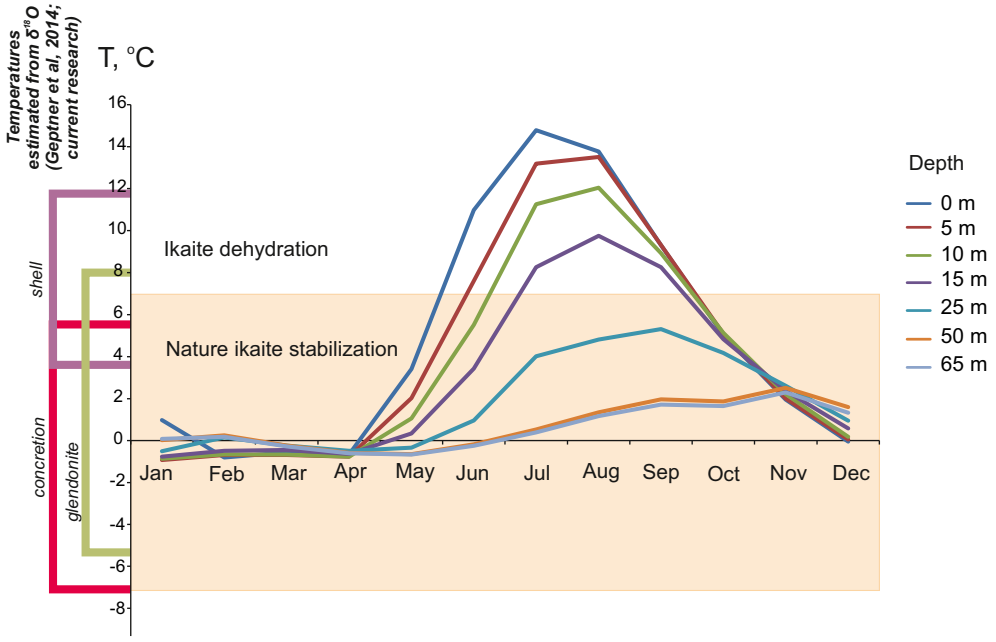

Fig. 12. Mean seawater temperatures in the White Sea from 1966 to 1999 (after Berger et al., 2003).

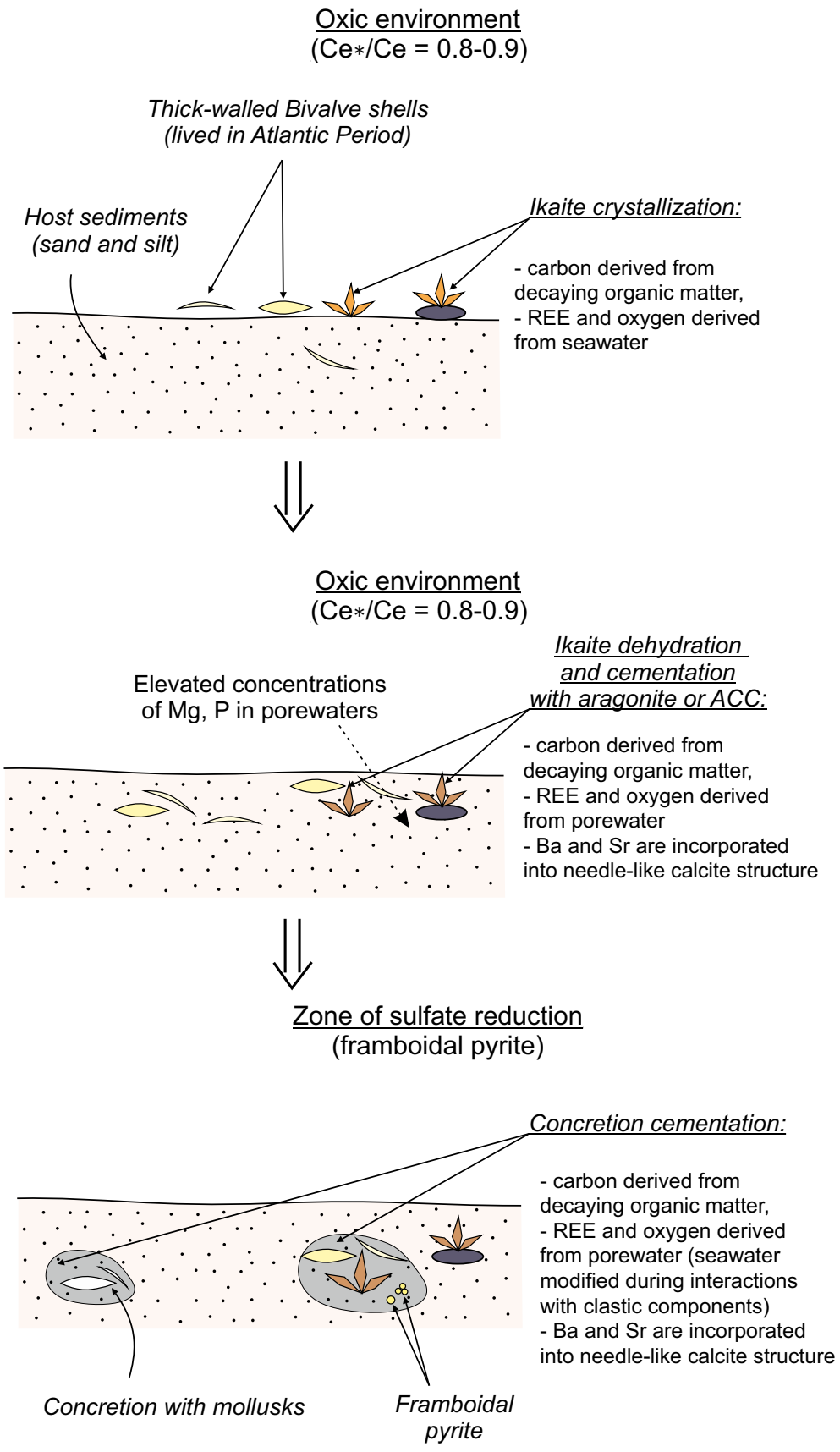

Fig. 13. Proposed model for ikaite precipitation, transformation and cementation during the Holocene in the White Sea.

pebbles (sample Fr-4; Fig. 2-2). Ikaite-derived calcite is depleted in Mg, Sr, Ba and P, which is probably determined by the ikaite crystal structure (e.g. (Hesse et al., 1983; Tateno and Kyono, 2014). PAAS-normalized REE patterns determined by LA-ICP-MS are characterized by a small negative Ce anomaly (0.8–0.9) and low superchondritic Y/Ho ratios (28–44; e.g., Bau, 1996; Nothdurft et al., 2004). The seawater that is characterized with negative Ce anomaly (Tostevin et al., 2016) and $\delta^{18}O$ values of dissolved inorganic carbon close to 0‰ PDB (Campbell, 2006) was probably the source of pore waters for ikaite crystallization, transformation and cementation of the host concretion. Small negative Ce anomaly and $\delta^{13}C$ values of −15 - -30‰ V-PDB indicate that carbon was derived during decomposition of organic matter (e.g. Campbell, 2006; Muramiya et al., 2022) in high alkalinity and high pH environments (Himmler et al., 2010; Hu et al., 2014).

PAAS-normalized REE specters of ikaite-derived calcite display comparable patterns to the needle-like cement (in terms of a small negative Ce anomaly and comparable Y/Ho ratio), but the amounts of Ba, Sr, Mg and P differ significantly. Higher concentrations of Ba and Sr could reflect precipitation of aragonite or amorphous calcium carbonate (ACC), which can both incorporate Mg, Ba and Sr (e.g., Saito et al., 2020; Stanienda, 2016).

Cementation of concretions occurred during sediment burial. The cementing calcite is rich in Mg, P, Ba and Sr, but at the same time displays almost flat PAAS-normalized REE-patterns, that reflects precipitation in clastic-dominated environment (e.g. Elderfield et al., 1990). The geochemical characteristics of the pore waters are determined by active ion-exchange with clastic material. Documented silicate's transformation in the early diagenesis of the modern White Sea sediments (Lein and Lisitsyn, 2018) and growing SiO_2 concentration in the sediments column supports the idea of geochemical changes in pore-water geochemistry through reactions with clastic material. Furthermore, the absence of a Ce anomaly and presence of framboidal pyrite crystals indicate cementation in a redox environment within the sulfate reduction zone.

7. Summary

The studied glendonites of the White Sea are composed of 2 to 3 calcite generations. The first generation of non-luminescent calcite is ikaite-derived and depleted in Mg, Sr and Ba. The second generation is micritic, P- and Mg-rich, with a dull red cathodoluminescence or is non-luminescent. The third generation comprises Mg, Sr and Ba-rich needle-like calcite with a dull red cathodoluminescence or is non-luminescent. The host concretion comprises sandstone cemented with high-magnesium calcite. The incorporation of Ba and Sr into carbonate phases is determined by their crystal structure. Ikaite cannot incorporate Mg, Ba and Sr, while aragonite and ACC have the capability to incorporate large cations (e.g., Sr and Ba).

Successive changes in $\delta^{13}C$ and PAAS-normalized REE specters indicate changes in the precipitation environment. Carbonate forming the bivalve shells yielded $\delta^{13}C$ values characteristic of DIC, a low Ce anomaly (0.3), Y/Ho ratios characteristic of seawater, and a depletion in HREE. The low Ce anomaly is indicative of precipitation in an oxic environment. Ikaite-derived calcite and needle-like cement are characterized by low $\delta^{13}C$ (up to −31.3‰ V-PDB), low negative Ce anomalies (0.8–0.9), low Y/Ho ratios (23–44) and high $^{87}Sr/^{86}Sr$ ratios. These results indicate that ikaite-derived calcite and needle-like cement crystallized in a high-alkalinity and high pH environment, from pore waters derived from seawater interacting with clastic material within the host sediments. Transformation of ikaite to calcite was probably driven by increasing temperatures. Calcite cementing the concretions is characterized by almost flat PAAS-normalized REE patterns and low (superchondritic) Y/Ho ratios (25–29), indicating that geochemistry of the calcite was determined by active ion-exchange between clastic sediments and pore waters in the sulfate-reduction zone.

The $^{230}Th/U$ age of the studied glendonites (4.1 ± 0.4 cal ka BP) indicates formation during the Subboreal Holocene Period. Estimated temperatures during glendonite formation range from −3.1 to +8 °C, suggesting that ikaite precipitation occurred during the cold winter months in the Subboreal Period when temperatures dropped below ~8 °C. Therefore, our data show that the formation of ikaite (and its pseudomorph glendonite) can be used as a proxy for low temperatures at least during the cold winter season.

Research data statement

Supplementary data to this article can be found online via link https://doi.org/10.5281/zenodo.6366977 or from KV k.vasilyeva@spbu.ru.

Declaration of Competing Interest

The authors declare that they have no known competing financial interests or personal relationships that could have appeared to influence the work reported in this paper.

Acknowledgements

The authors acknowledge the Resource Center of X-ray diffraction studies and "Geomodel" Resource Centre of Saint-Petersburg State University for providing instrumental and computational resources. The reequipment and comprehensive development of the "Geoanalitik" shared research facilities of the IGG UB RAS is financially supported by the grant of the Ministry of Science and Higher Education of the Russian Federation for 2021-2023 (Agreement No. 075-15-2021-680). Mineralogical studies were supported by the Council for Grants of the President of the Russian Federation No NSh-1462.2022.1.5 (for OV and IC). This study has been carried out following the plans of the scientific research of the Geological Institute of RAS (for NZ, VE and MR); the overview of the White Sea history in the Holocene was conducted within the frame of the IG RAS state assignment FMWS-2019-0008 (NZ) partly supported be RSF grant 22-17-00081. The authors are very grateful to Editor-in-Chief, Dr. Adina Paytan and to both anonymous reviewers for constructive criticism and useful comments on manuscript content. Special thanks to James Barnet, (Camborne School of Mines) for editing the English.

Appendix A. Supplementary data

Supplementary data to this article can be found online at https://doi.org/10.1016/j.margeo.2022.106820.

References

Agafonova, E., Polyakova, Y., Novichkova, Y., 2020. The diatom response to Postglacial environments in the White Sea, the European Arctic. Mar. Micropaleontol. 161, 101927 https://doi.org/10.1016/j.marmicro.2020.101927.

Astafiev, B.Yu., Bogdanov, Yu.B., Voiova, O.A., Voinov, A.S., et al., 2012. State geological map of tha Russian Federation. Scale 1: 1 000 000 (the 3rd generation). Baltic Series. Map Q-37 Archangel'sk (in Russian). Explanationary note. St. Petersburg, St. Petersburg Cartographic Factory, p. 302.

Bau, M., 1996. Controls on the fractionation of isovalent trace elements in magmatic and aqueous systems: evidence from Y/Ho, Zr/Hf, and lanthanide tetrad effect. Contrib. Mineral. Petrol. 123, 323–333. https://doi.org/10.1007/s004100050159.

Bau, M., Alexander, B., 2006. Preservation of primary REE patterns without Ce anomaly during dolomitization of Mid-Paleoproterozoic limestone and the potential re-establishment of marine anoxia immediately after the"Great Oxidation Event.". South Afr. J. Geol. 109, 81–86. https://doi.org/10.2113/gssajg.109.1-2.81.

Bau, M., Dulski, P., 1996. Distribution of yttrium and rare-earth elements in the Penge and Kuruman iron-formations, Transvaal Supergroup, South Africa. Precambrian Res. 79, 37–55.

Bazarova, E.P., Kadebskaya, O.I., 2019. Cryogenic mineral formations in the caves of priolkhonie region (Western Pribaikalye). Earths Cryosphere 23, 8–18. https://doi.org/10.21782/KZ1560-7496-2019-6(8-18).

Bazarova, E.P., Kononov, A.M., Gutareva, O.S., Nartova, N.V., 2014. Characteristics of cryogenic mineral formations of Okhotnichya Cave at Pre-Baikal areas (Irkutsk region). Earths Cryosphere XVIII 67–76 (in Ruusian).

Bazarova, E.P., Kadebskaya, O.I., Kononov, A.M., Ushchapovskaya, Z.F., 2016. Conditions and characteristics of cryogenic mineral formation in the caves of

Southern part of Siberian platform folding margins (Western Pre-Baikal Region and Eastern Sayan). Bull. Perm Univ. Geol. 2, 22–34. https://doi.org/10.17072/psu.geol.30.22.

Bazarova, E.P., Kadebskaya, O.I., Tsurikhin, E.A., 2018. Cryogenic minerals in caves of the Vizhay River (Northern Urals). Bull. Perm Univ. 17, 11–17. https://doi.org/10.17072/psu.geol.17.1.11.

Berger, V. ÍA͡, Smolyar, I., Levitus, Sydney, Tatusko, R., Zoologicheskiĭ institut (Rossiĭskaĭa͡akademiĭa͡nauk), National Oceanographic Data Center (U.S.). Ocean Climate Laboratory, 2003. 36-year time series (1963-1998) of zooplankton, temperature, and salinity in the White Sea. Silver Spring, Md. : St. Petersburg : U.S. Dept. of Commerce, National Oceanic and Atmospheric Administration, National Environmental Satellite, Data, and Information Service [National Oceanographic Data Center, Ocean Climate Laboratory]. Russian Academy of Sciences, Zoological Institute. http://purl.access.gpo.gov/GPO/LPS50937.

Bischoff, J.L., Fitzpatrick, J.A., 1991. U-series dating of impure carbonates: an isochron technique using total-sample dissolution. Geochim. Cosmochim. Acta 55, 543–554.

Campbell, K.A., 2006. Hydrocarbon seep and hydrothermal vent paleoenvironments and paleontology: past developments and future research directions. Palaeogeogr. Palaeoclimatol. Palaeoecol. 232, 362–407. https://doi.org/10.1016/j.palaeo.2005.06.018.

Derkachev, A.N., Nikolaeva, N.A., Mozherovsky, A.V., Grigor'eva, T.N., Ivanova, E.D., Pletnev, S.P., Barinov, N.N., Chubarov, V.M., 2007. Mineralogical and geochemical indicators of anoxic sedimentation conditions in local depressions within the Sea of Okhotsk in the late Pleistocene-Holocene. Russ. J. Pac. Geol. 1, 203–229. https://doi.org/10.1134/S1819714007030013.

Dieckmann, G.S., Nehrke, G., Papadimitriou, S., Göttlicher, J., Steininger, R., Kennedy, H., Wolf-Gladrow, D., Thomas, D.N., 2008. Calcium carbonate as ikaite crystals in Antarctic Sea ice. Geophys. Res. Lett. 35, 35–37. https://doi.org/10.1029/2008GL033540.

Domack, E.W., Halverson, G., Willmott, V., Leventer, A., Brachfeld, S., Ishman, S.E., 2007. Spatial and temporal distribution of Ikaite crystals in Antarctic glacial marine sediments. In: Cooper, A.K., Raymond, C.R. (Eds.), Online Proceedings of the 10th ISAES X, pp. 2–6.

El Meknassi, S., Dera, G., Cardone, T., De Rafélis, M., Brahmi, C., Chavagnac, V., 2018. Sr isotope ratios of modern carbonate shells: good and bad news for chemostratigraphy. Geology 46, 1003–1006. https://doi.org/10.1130/G45380.1.

Elderfield, H., Upstill-Goddard, R., Sholkovitz, E.R., 1990. The rare earth elements in rivers, estuaries, and coastal seas and their significance to the composition of ocean waters. Geochim. Cosmochim. Acta 54, 971–991. https://doi.org/10.1016/0016-7037(90)90432-K.

Fedotova, M.G., Voloshin, A.V., Vetrin, V.R., 1986. Speaking of glendonites. In: Geochemical Research in Forest and Tundra Landscapes, pp. 137–144 (in Russian).

Fersman, A.E., 1938. Geochemistry and mineralogy of Polar regions. Proc. Acad. Sci. USSR XIX 623–626 (in Russian).

Geptner, A.R., Pokrovsky, B.G., Sadchikova, T.A., Sulerzhitsky, L.D., Chernyakhovsky, A.G., 1994. Local carbonatization of sediments of the White Sea (concept of microbiological formation). Lithol. Miner. Resour. 3–22.

Geptner, A.R., Vetoshkina, O.S., Petrova, V.V., 2014. New data on the composition of stable isotopes in glendonites of the White Sea and their genesis. Lithol. Miner. Resour. 49, 473–490. https://doi.org/10.1134/S0024490214060042.

Geyh, M.A., 2008. Selection of suitable data sets improves 230Th/U dates of dirty material. Geochronometria 30, 69–77.

Govberg, L.I., 1968. Mollusks distribution in the thickness of the Holocene sediments of the Onega Bay. Oceanology 8, 666–679 (in Russian).

Govberg, L.I., 1970. Mollusks distribution in the thickness of the Holocene sediments of the White Sea. Oceanology 10, 837–848 (in Russian).

Greinert, J., Derkachev, A., 2004. Glendonites and methane-derived Mg-calcites in the Sea of Okhotsk, Eastern Siberia: implications of a venting-related ikaite/glendonite formation. Mar. Geol. 204, 129–144. https://doi.org/10.1016/S0025-3227(03)00354-2.

Hesse, K.-F., Küppers, H., Suess, E., 1983. Refinement of the structure of Ikaite, $CaCO_3 \cdot 6H_2O$. Z. Für Krist. - Cryst. Mater. 163, 227–231. https://doi.org/10.1524/zkri.1983.163.3-4.227.

Himmler, T., Bach, W., Bohrmann, G., Peckmann, J., 2010. Rare earth elements in authigenic methane-seep carbonates as tracers for fluid composition during early diagenesis. Chem. Geol. 277, 126–136. https://doi.org/10.1016/j.chemgeo.2010.07.015.

Hu, Y. Bin, Wolf-Gladrow, D.A., Dieckmann, G.S., Völker, C., Nehrke, G., 2014. A laboratory study of ikaite (CaCO3·6H2O) precipitation as a function of pH, salinity, temperature and phosphate concentration. Mar. Chem. 162, 10–18. https://doi.org/10.1016/j.marchem.2014.02.003.

Huggett, J.M., Schultz, B.P., Shearman, D.J., Smith, A.J., 2005. The petrology of ikaite pseudomorphs and their diagenesis. Proc. Geol. Assoc. 116, 207–220. https://doi.org/10.1016/S0016-7878(05)80042-2.

Hughes, A.L.C., Gyllencreutz, R., Lohne, Ø.S., Mangerud, J., Svendsen, J.I., 2016. The last Eurasian ice sheets - a chronological database and time-slice reconstruction, DATED-1. Boreas 45, 1–45. https://doi.org/10.1111/bor.12142.

Jeremejew, P., 1882. Die pseudomorphen Krystalle des Aragonite und des Eisen-oxydes ans den russischen Fundorten. Verhandlungen Russ.-Kais. Mineral. Ges. Zu St Petersburg 2, 319–336.

Jochum, K.P., Nohl, U., Herwig, K., Lammel, E., Stoll, B., Hofmann, A.W., 2005. GeoReM: a new geochemical database for reference materials and isotopic standards. Geostand. Geoanal. Res. 29, 333–338. https://doi.org/10.1111/j.1751-908X.2005.tb00904.x.

Jon, D. Woodhead, John Hellstrom, Janet, M. Hergt, Alan Greig, Roland Maas, 2007. Isotopic and Elemental Imaging of Geological Materials by Laser Ablation Inductively Coupled Plasma-Mass Spectrometry. Geostand. Geoanal. Res. 31 (4), 331–343. https://doi.org/10.1111/j.1751-908X.2007.00104.x.

Kaplan, M.E., 1979. Calcite pseudomorphs (pseudogaylussite, jarrowite, thinolite, glendonite, gennoishi, White Sea hornlets) in sedimentary rocks. Review of major localities. Lithol. Miner. Resour. 5, 125–141.

Kaplan, M.E., 1980. Calcite pseudomorphs (pseudogaylussite, jarrowite, thinolite, glendonite, gennoishi, White Sea hornlets) in sedimentary rocks: origins of the pseudomorphs. Lithol. Miner. Resour. 14, 623–636.

Killam, D.E., Clapham, M.E., 2018. Identifying the ticks of bivalve shell clocks: seasonal growth in relation to temperature and food supply. PALAIOS 33, 228–236. https://doi.org/10.2110/palo.2017.072.

Kim, S.T., O'Neil, J.R., 1997. Equilibrium and nonequilibrium oxygen isotope effects in synthetic carbonates. Geochim. Cosmochim. Acta 61, 3461–3475. https://doi.org/10.1016/S0016-7037(97)00169-5.

Kodina, L.A., Tokarev, V.G., Sukhomk, V.J., Vlasova, L.N., Pribylova, T.N., 2001. Preliminary results of geochemical investigations of sediment 179 cores along the Yenisei Profile (Acoustic Units I - II). In: Stein, R., Stepanets, O. (Eds.), The German-Russian Project on Siberian River Run-off (SIRRO): Scientific Cruise Report of the Kara-Sea Expedition "SIRRO 2000" of RV "Akademik Boris Petrov" and First Results. Ber. Polarforsch. Meeresforsch, p. 286.

Kolka, V.V., Yevzerov, V.Ya., Moller, J.J., Corner, G.D., 2013. The Late Weichselian and Holocene relative sea-level change and isolation basin stratigraphy at the Umba settlement, southern coast of Kola Peninsula. Izv. RAS Geogr. Ser. 794, 73–88 (in Russian).

Koshechkin, B.I., 1979. Holocene tectonic of the Eastern part of the Baltic shield (in Russian). Leningrad, Nauka, p. 160.

Krylov, A.A., Logvina, E.A., Matveeva, T.M., Prasolov, E.M., Sapega, V.F., Demidova, A.L., Radchenko, M.S., 2015. IKAITE (CaCO36H2O) IN BOTTOM SEDIMENTS OF THE LAPTEVS' SEA AND THE ROLE OF ANAEROBIC METHANE OXIDATION IN THIS MINERAL-FORMING PROCESS. Zapiski RMO 61–75.

Last, F.M., Last, W.M., Fayek, M., Halden, N.M., 2013. Occurrence and significance of a cold-water carbonate pseudomorph in microbialites from a saline lake. J. Paleolimnol. 50, 505–517. https://doi.org/10.1007/s10933-013-9742-6.

Lavrova, M.A., 1960. Quaternary Geology of the Kola Peninsula. Moscow-St, Petersburg (in Russian).

Lein, A.Yu., Lisitsyn, A.P., 2018. Processes of early diagenesis in the Arctic Seas (on the example of the White Sea). In: Lisitsyn, A.P., Demina, L.L. (Eds.), Sedimentation Processes in the White Sea, the Handbook of Environmental Chemistry. Springer International Publishing, Cham, pp. 165–206. https://doi.org/10.1007/698_2018_345.

Maksimov, F.E., Kuznetsov, V.Y., 2010. New version of the 230Th/U dating method of the Upper and Middle Neopleistocene deposits. Vestn. St Petersburg State Univ. 7, 94–107 (in Russian).

McArthur, J.M., Howarth, R.J., Bailey, T.R., 2001. Strontium isotope stratigraphy: LOWESS version 3: best fit to the marine Sr-isotope curve for 0–509 Ma and accompanying look-up table for deriving numerical age. J. Geol. 109, 155–170. https://doi.org/10.1086/319243.

Morales, C., Rogov, M., Wierzbowski, H., Ershova, V., Suan, G., Adatte, T., Föllmi, K.B., Tegelaar, E., Reichart, G.J., de Lange, G.J., Middelburg, J.J., van de Schootbrugge, B., 2017. Glendonites track methane seepage in Mesozoic polar seas. Geology 45, 503–506. https://doi.org/10.1130/G38967.1.

Muramiya, Y., Yoshida, H., Minami, M., Mikami, T., Kobayashi, T., Sekiuchi, K., Katsuta, N., 2022. Glendonite concretion formation due to dead organism decomposition. Sediment. Geol. 429, 106075 https://doi.org/10.1016/j.sedgeo.2021.106075.

Naumov, A.D., 2006. Clams of the White Sea. Ecological and Faunistic Analysis. Russian Academy of Sciences, St Petersburg (in Russian).

Nevessky, E.N., Medvedev, V.S., Kalinenko, V.V., 1977. White Sea: Sedimentogenesis and History of Development in the Holocene. Nauka, Moscow (in Russian).

Nothdurft, L., Webb, G., Kamber, B., 2004. Rare earth element geochemistry of Late Devonian reefal carbonates, Canning Basin, Western Australia: confirmation of a seawater REE proxy in ancient limestones. Geochim. Cosmochim. Acta 68, 263–283. https://doi.org/10.1016/S0016-7037(03)00422-8.

Novichkova, Y.A., Reikhard, L.Y., Lisitzin, A.P., Rybalko, A.Y., de Vernal, A., 2017. New data on the Holocene evolution of the Dvina Bay (White Sea). Dokl. Earth Sci. 474, 607–611. https://doi.org/10.1134/S1028334X17050233.

Obzhirov, A.I., Astakhov, A.S., Astakhova, N.V., 2000. Genesis and conditions for the formation of avtigenetic carbonates in the Gvartenary sediments layer in the region of the Sakhalin-Deryugin gas anomaly in the Okhotsk Sea. Oceanology 40, 280–288 (in Russian).

Ponnurangam, A., Bau, M., Brenner, M., Koschinsky, A., 2016. Mussel shells of Mytilus edulis as bioarchives of the distribution of rare earth elements and yttrium in seawater and the potential impact of pH and temperature on their partitioning behavior. Biogeosciences 13, 751–760. https://doi.org/10.5194/bg-13-751-2016.

Price, G.D., 1999. The evidence and implications of polar ice during the Mesozoic. Earth-Sci. Rev. 48, 183–210. https://doi.org/10.1016/S0012-8252(99)00048-3.

Repkina, T. Yu, Zaretskaya, N.E., Subetto, D.A., Potakhin, M.S., Qungaa, M. Ch., Novikova, A.V., Leont'ev, P.A., 2018. COASTAL MORPHODYNAMICS OF THE NORTH-WESTERN ONEZHSKY PENINSULA, WHITE SEA IN THE HOLOCENE. KONYUKHOV BAY (in Russian). Proceedings of the Karelian research centre of the Russian academy of sciences 1, 3–22.

Rogov, M.A., Ershova, V.B., Shchepetova, E.V., Zakharov, V.A., Pokrovsky, B.G., Khudoley, A.K., 2017. Earliest Cretaceous (late Berriasian) glendonites from Northeast Siberia revise the timing of initiation of transient Early Cretaceous cooling in the high latitudes. Cretac. Res. 71, 102–112. https://doi.org/10.1016/j.cretres.2016.11.011.

Rogov, M., Ershova, V., Vereshchagin, O., Vasileva, K., Mikhailova, K., Krylov, A., 2021. Database of global glendonite and ikaite records throughout the Phanerozoic. Earth Syst. Sci. Data 13, 343–356. https://doi.org/10.5194/essd-13-343-2021.

Rosalie, Tostevin, Graham, A. Shields, Gary, M. Tarbuck, Tianchen, He, Matthew, O. Clarkson, Rachel, A. Wood, 2016. Effective use of cerium anomalies as a redox proxy in carbonate-dominated marine settings. Chem. Geol. 438, 146–162. https://doi.org/10.1016/j.chemgeo.2016.06.027. ISSN 0009-2541. https://www.sciencedirect.com/science/article/pii/S0009254116303278.

Rowe, P.J., Maher, B.A., 2000. 'Cold' stage formation of calcrete nodules in the Chinese Loess Plateau: evidence from U-series dating and stable isotope analysis. Palaeogeogr. Palaeoclimatol. Palaeoecol. 157, 109–125.

Saito, A., Kagi, H., Marugata, S., Komatsu, K., Enomoto, D., Maruyama, K., Kawano, J., 2020. Incorporation of incompatible strontium and barium. Minerals 10, 270.

Schultz, B.P., 2009. Pseudomoroh after ikaite – called Glendonite is it a geological thermometer in cold sediments or geological oddity as it occurs close to PETM in the Fur formation. IOP Conf. Ser. Earth Environ. Sci. 6, 072059 https://doi.org/10.1088/1755-1307/6/7/072059.

Sokolov, D., 1825. On White Sea mineral. Min. J. Gorny Zhurnal 117–120 (in Russian).

Stanienda, K., 2016. Strontium and barium in the triassic limestone of the Opole Silesia deposits. Arch. Min. Sci. 61, 29–46. https://doi.org/10.1515/amsc-2016-0003.

Subetto, D.A., Shevchenko, V.P., Ludikova, A.V., Kuznetsov, D.D., Sapelko, T.V., Lisitsyn, A.P., Evzerov, V. Ya., van Beek, P., Suo, M., Subetto, G.D., 2012. The chronology of isolation of the Solovetsky Archipelago lakes and current rates of lake sedimentation. DAN [Dokl Earth Sciences] 446 (2), 183–190.

Suess, E., Balzer, W., Hesse, K., Müller, P., Ungerer, C., Wefer, G., 1982. Calcium carbonate hexahydrate from organic-Rich sediments of the Antarctic shelf: precursors of glendonites. Science 216, 1128–1131. https://doi.org/10.1126/science.216.4550.1128.

Tateno, N., Kyono, A., 2014. Structural change induced by dehydration in ikaite (CaCO3·6H2O). J. Mineral. Petrol. Sci. 109, 157–168. https://doi.org/10.2465/jmps.140320.

Taylor, S.R., McLennan, S.M., 1985. The Continental Crust: Its Composition and Evolution. Blackwell Scientific Publications, Palo Alto.

Teichert, B.M.A., Luppold, F.W., 2013. Glendonites from an Early Jurassic methane seep — climate or methane indicators? Palaeogeogr. Palaeoclimatol. Palaeoecol. 390, 81–93. https://doi.org/10.1016/j.palaeo.2013.03.001.

Tollefsen, E., Balic-Zunic, T., Mörth, C.M., Brüchert, V., Lee, C.C., Skelton, A., 2020. Ikaite nucleation at 35 °C challenges the use of glendonite as a paleotemperature indicator. Sci. Rep. 10, 1–10. https://doi.org/10.1038/s41598-020-64751-5.

Vasileva, K., Rogov, M., Ershova, V., Pokrovsky, B., 2019. New results of stable isotope and petrographic studies of Jurassic glendonites from Siberia View supplementary material New results of stable isotope and petrographic studies of Jurassic glendonites from Siberia. Gff -Upps. https://doi.org/10.1080/11035897.2019.1641549.

Vickers, M., Watkinson, M., Price, G., Jerrett, R., 2018. An improved model for the ikaite-glendonite transformation: evidence from the Lower Cretaceous of Spitsbergen. Svalbard. Nor. J. Geol. 98 https://doi.org/10.17850/njg98-1-01.

Vickers, M.L., Lengger, S.K., Bernasconi, S.M., Thibault, N., Schultz, B.P., Fernandez, A., Ullmann, C.V., Mccormack, P., Bjerrum, C.J., Rasmussen, J.A., Hougård, I.W., Korte, C., 2020. Cold spells in the Nordic Seas during the early Eocene Greenhouse. Nat. Commun. 11, 1–12. https://doi.org/10.1038/s41467-020-18558-7.

Whiticar, M.J., Suess, E., 1998. The cold carbonate connection between Mono Lake, California and the Bransfield Strait, Antarctica. Aquat. Geochem. 429–454. https://doi.org/10.1023/A:1009696617671.

Zabel, M., Schulz, H.D., 2001. Importance of submarine landslides for non-steady state conditions in pore water systems — lower Zaire (Congo) deep-sea fan. Mar. Geol. 176, 87–99. https://doi.org/10.1016/S0025-3227(01)00164-5.

Zaitsev, A.V., Pokrovsky, B.G., 2014. Carbon and oxygen isotope compositions of Lower-Middle Ordovician carbonate rocks in the northwestern Russian platform. Lithol. Miner. Resour. 49, 283–291. https://doi.org/10.1134/S0024490214030079.

Zaretskaya, N.E., Ludikova, A.V., Shvarev, S.V., Kuznetsov, D.D., Kutenkov, S.A., 2020. Palaeoseismic fault trenches as unique archives of the White Sea Holocene history. Geomorphologia 4, 45–57. https://doi.org/10.31857/S0435428120040112.

Zaretskaya, N., Rybalko, A., Repkina, T., Shilova, O., Krylov, A., 2021. Late Pleistocene in the southeastern White Sea and adjacent areas (Arkhangelsk region, Russia): stratigraphy and palaeoenvironments. Quat. Int. 605–606, 126–141. https://doi.org/10.1016/j.quaint.2020.10.057.